BIOCHEMISTRY
including biophysical chemistry & molecular biology
Article

Biochemistry **2010,** *49,* 3815–3823 3815
DOI: 10.1021/bi902214j

Probing Soluble Guanylate Cyclase Activation by CO and YC-1 Using Resonance Raman Spectroscopy[†]

Mohammed Ibrahim,[‡] Emily R. Derbyshire,[§] Michael A. Marletta,[§,∥] and Thomas G. Spiro*[,‡]

[‡]*Department of Chemistry, University of Washington, Seattle, Washington 98195-1700,* [§]*Department of Molecular and Cell Biology, University of California, Berkeley, California 94720-3220, and* [∥]*Department of Chemistry, University of California, Berkeley, California 94720-3220*

Received December 28, 2009; Revised Manuscript Received March 29, 2010

ABSTRACT: Soluble guanylate cyclase (sGC) is weakly activated by carbon monoxide (CO) but is significantly activated by the binding of YC-1 to the sGC−CO complex. In this report, resonance Raman (RR) spectroscopy was used to study selected sGC variants. Addition of YC-1 to the sGC−CO complex alters the intensity pattern of RR bands assigned to the vinyl and propionate heme substituents, suggesting changes in the tilting of the pyrrole rings to which they are attached. YC-1 also shifts the RR intensity of the ν_{FeC} and ν_{CO} bands from 473 and 1985 cm^{-1} to 487 and 1969 cm^{-1}, respectively, and induces an additional ν_{FeC} band, at 521 cm^{-1}, assigned to five-coordinate heme-CO. Site-directed variants in the proximal heme pocket (P118A) or in the distal heme pocket (V5Y and I149Y) reduce the extent of YC-1 activation, along with the 473 cm^{-1} band intensity. These lower-activity sGC variants display another ν_{FeC} band at 493 cm^{-1} which is insensitive to YC-1 addition and is attributed to protein that cannot be activated by the allosteric activator. The results are consistent with a model in which YC-1 binding to the sGC−CO complex results in a conformational change that activates the protein. Specifically, YC-1 binding alters the heme geometry via peripheral nonbonded contacts and also relieves an intrinsic electronic effect that weakens FeCO back-bonding in the native, YC-1 responsive protein. This electronic effect might involve neutralization of the heme propionates via H-bond contacts or negative polarization by a distal cysteine residue. YC-1 binding also strains the Fe−histidine bond, leading to a population of the five-coordinate sGC−CO complex in addition to a conformationally distinct population of the six-coordinate sGC−CO complex. The loss of YC-1 activation in the sGC variants might involve a weakening of the heme−protein contacts that are thought to be critical to a YC-1-induced conformational change.

Soluble guanylate cyclase (sGC)[1] is the key transducer of nitric oxide (NO) signaling in biology (*1*). In mammals, an array of physiological responses are activated when sGC produces the second-messenger cyclic GMP (cGMP) in response to NO binding (*1*, *2*).

In addition to NO, sGC binds carbon monoxide (CO), and there is much interest in the possibility that CO might be a physiologically relevant signaling molecule (*3*−*5*). sGC is activated to a small extent by CO, but addition of the synthetic effector molecules YC-1 or BAY 41-2272 to the sGC−CO complex significantly increases sGC activity (*6*). It has recently been reported that the stoichiometric binding of NO to sGC (1-NO) also generates a low-activity species (*7*, *8*). Like the low-activity sGC−CO complex, the low-activity sGC−NO complex is significantly activated in the presence of YC-1 (*8*, *9*). However, excess NO produces a high-activity form of sGC by binding to a non-heme site involving cysteine residues (*10*), a mechanism not available to CO.

sGC is a heterodimeric protein consisting of an α1 subunit and a β1 subunit. The β1 subunit consists of Heme-Nitric oxide/OXygen (H-NOX), PAS, CC (coiled-coil), and catalytic domains (Figure 1). The heme cofactor is bound to the β1 H-NOX domain, which is a conserved domain with a unique structure (*11*). To date, three wild-type H-NOX domain crystal structures have been reported (*12*−*14*). Figure 2 shows a homology model of this domain in sGC based on the crystal structure of the H-NOX domain of a bacterial [*Thermoanaerobacter tengcongensis* (*Tt*)] chemoreceptor protein (*14*). The heme is attached to the protein through the proximal His105 side chain (His102 in *Tt* H-NOX), and a number of peripheral nonbonded contacts. The heme is sandwiched between the proximal and distal halves of the protein, whose relative orientations are somewhat variable in different molecules of the *Tt* H-NOX unit cell. Of particular note is the observation that the P115A substitution (P118A in rat sGC β1) relaxes the highly distorted heme geometry found in *Tt* H-NOX and induces a substantial reorientation of the distal (N-terminal) half of the domain (*15*). This structural change suggests a pathway for transmission of the signal from the heme to the functional domain (*16*). Additionally, ligation of *Nostoc* sp. (*Ns*) H-NOX by NO or CO produces a similar intradomain reorientation (*12*).

[†]This work was supported financially by National Institutes of Health Grants GM033576 (T.G.S.) and GM077365 (M.A.M.).

*To whom correspondence should be addressed. Phone: (206) 685-4964. Fax: (206) 685-8665. E-mail: spiro@chem.washington.edu.

[1]Abbreviations: sGC, soluble guanylate cyclase; CO, carbon monoxide; NO, nitric oxide; YC-1, 3-(5′-hydroxymethyl-3′-furyl)-1-benzylindazole; RR, resonance Raman; cGMP, cyclic guanosine 3′,5′-monophosphate; BAY 41-2272, 5-cyclopropyl-2-[1-(2-fluorobenzyl)-1*H*-pyrazolo[3,4-*b*]-pyridin-3-yl]pyrimidin-4-ylamine; H-NOX, Heme-Nitric oxide/OXygen binding; *Tt*, *Thermoanaerobacter tengcongensis*; *Ns*, *Nostoc* sp.; HEPES, 4-(2-hydroxyethyl)-1-piperazineethanesulfonic acid; DTT, dithiothreitol; GTP, guanosine 5′-triphosphate; DMSO, dimethyl sulfoxide; Ti:sapphire, titanium sapphire; Nd:YLF, neodymium-doped yttrium lithium fluoride; CCD, charge-coupled device; WT, wild type; 6-c, six-coordinate; 5-c, five-coordinate; UVRR, ultraviolet resonance Raman; DFT, density functional theory; NMR, nuclear magnetic resonance; PDB, Protein Data Bank.

Published on Web 03/30/2010

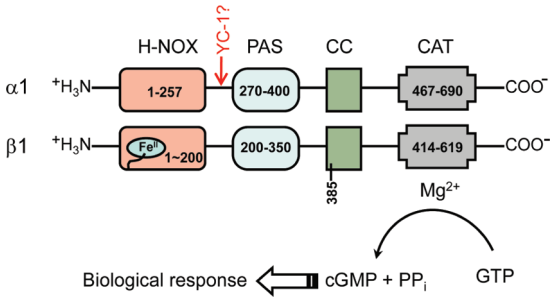

FIGURE 1: Domain structure of sGC (adapted from ref *1*). The H-NOX, PAS, CC (coiled-coil), and catalytic (CAT) domains are shown.

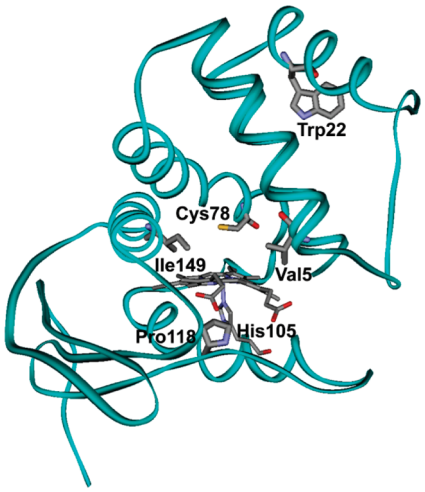

FIGURE 2: Homology model of the rat sGC β1 H-NOX domain [based on the *Tt* H-NOX structure (PDB entry 1U55)].

The binding site for YC-1 is uncertain. Mutational studies had suggested that YC-1 interacts with the catalytic domain (*17*), but recent biochemical experiments rule this out (*18*). There is an effector site on the catalytic domain, but it binds nucleotides and not YC-1 (*18*). Photoaffinity studies with YC-1 analogues have found a label on the sGC α1 subunit, specifically at Cys238 and Cys243 (*19*). This finding suggests that YC-1 binds within the linker region between the H-NOX and PAS domains (Figure 1), a proposal that is supported by a study showing elimination of YC-1 activation upon deletion of residues 259−364 from the α1 chain (*20*). Also, YC-1 binding has been shown to occur in the N-terminal two-thirds of sGC from *Manduca sexta* (*21*, *22*). Thus, YC-1 likely exerts its effect through an allosteric interaction from a site remote to both the heme and the catalytic center.

In this study, we seek to elucidate the YC-1 effect using visible and ultraviolet (UV) resonance Raman spectroscopic methods to probe both the changes in the heme structure and the environment of aromatic residues. YC-1 is found to impose changes in the heme geometry, the status of the Fe−His bond, the electronic structure of bound CO, and the environment around aromatic residues of the β1 subunit. The CO effect is used to show that residue substitutions in the heme pocket that weaken YC-1 activation also reduce the magnitude of the spectroscopic signal in proportion. These observations support and extend previous results from the laboratories of Kitagawa (*23*) and Kincaid (*24*). On the basis of our findings, we suggest a model in which YC-1 binding induces a protein conformational change that exerts a torque on the heme, and this YC-1-induced movement is vitiated when the protein−heme contacts are perturbed by activity-impairing residue substitutions.

METHODS

Protein Expression, Purification, and Activity Assay. Rat sGC α1β1 was purified as described previously (*25*). Rat β1(1−194) and β1(1−385) were purified according to a previously published protocol (*11*). β1(1−194) variant P118A and full-length β1 variants V5Y, P118A, and I149Y were generated and purified by a method that will be described elsewhere. Additionally, β1(1−194) P118A and α1β1 P118A were purified without heme and reconstituted according to a method that will be described elsewhere.

The activity of α1β1 variants V5Y, P118A, and I149Y was measured in the presence and absence of YC-1 (Cayman Chemical) and CO. CO(g) was added to sGC (233 nM) in 50 mM HEPES (pH 7.4) and 50 mM NaCl in an anaerobic cuvette. After formation of the complex had been confirmed by UV−vis spectroscopy, the protein was added to an assay mixture to initiate the enzyme reaction. The final assay contained 0.2 μg of enzyme in 50 mM HEPES (pH 7.4), 1 mM DTT, 3 mM $MgCl_2$, 1.5 mM GTP, and 150 μM YC-1 where indicated. All assays were conducted in a final volume of 100 μL and had a concentration of 2% DMSO, which was shown not to affect enzyme activity. Reactions were quenched after 3 min by the addition of 400 μL of 125 mM $Zn(CH_3CO_2)_2$ and 500 μL of 125 mM Na_2CO_3. cGMP quantification was conducted using a cGMP enzyme immunoassay kit, Format B (Biomol), per the manufacturer's instructions. Each experiment was repeated two to four times to ensure reproducibility.

Resonance Raman (RR) Spectroscopy. sGC−CO samples for visible RR experiments were prepared by passing high-purity CO gas through ligand-free sGC samples [4−10 μM in 50 mM HEPES (pH 7.4), 50 mM NaCl, and 1 mM DTT] in a septum-sealed NMR tube for ~15 min. Formation of the Fe(II)−CO adduct was confirmed by UV−vis spectroscopy. For UVRR experiments, β1(1−385)−CO samples were prepared in the same manner, except that the protein concentration was higher (50 μM) and the samples contained 0.2 M sodium perchlorate as an internal standard. YC-1 (Cayman Chemical)-bound and BAY 41-2272 (Cayman Chemical)-bound samples were prepared by addition of YC-1 and BAY 41-2272 stocks in DMSO anaerobically to the CO-bound sample, yielding final YC-1 and BAY 41-2272 concentrations of 100−150 μM [~2% (v/v) DMSO].

RR spectra were recorded for samples in spinning NMR tubes via backscattering geometry at room temperature. For visible RR experiments, the excitation wavelengths at 430 nm (for ligand-free samples) and 413 nm (for CO-bound samples) were obtained by frequency doubling, using a nonlinear lithium triborate crystal, of a Ti:sapphire laser (Photonics International TU-UV), which was pumped by the second harmonic of a Q-switched Nd:YLF laser (Photonics Industries International, GM-30-527). The laser power at the sample was kept to a minimum (<1 mW) by using a cylindrical lens to prevent photolysis of bound CO. Scattered light was collected and focused onto a single spectrograph (SPEX 1269) equipped with a CCD detector (Roper Scientific) operating at −110 °C. Spectra were calibrated with dimethylformamide and DMSO. For UVRR experiments, samples were excited at 229 nm from an intracavity doubled-argon ion laser (Innova 300 FReD, Coherent Radiation). Sample degradation was minimized

Table 1: Effect of YC-1 on the sGC−CO Activity Levels and the ~473 cm^{-1} RR Band Intensity

	specific activity (nmol min^{-1} mg^{-1})				$\%A_{473}$		
sGC	without YC-1	with YC-1	Δactivity[a] (nmol min^{-1} mg^{-1})	Δactivity (%)[b]	without YC-1	with YC-1	$\Delta(\%A)_{473}$[c]
CO-free WT	13 ± 2.4	86 ± 65	73	7.2	–	–	–
WT	134 ± 20	1143 ± 98	1009	100	36.5	12.7	23.8
P118A	18 ± 5.1	369 ± 91	351	34.8	10.8	0	10.8
V5Y	43 ± 0.3	423 ± 90	380	37.7	7.9	0	7.9
I149Y	250 ± 82	185 ± 61	0	0	0	0	0

[a] Δactivity = (specific activity)$_{+YC-1}$ − (specific activity)$_{-YC-1}$. [b] Δactivity (%) = (Δactivity)$_{variant}$/(Δactivity)$_{WT}$ × 100. [c] $\Delta(\%A)_{473} = [(A_{473}/A_{total})_{-YC-1} - (A_{473}/A_{total})_{+YC-1}] \times 100$.

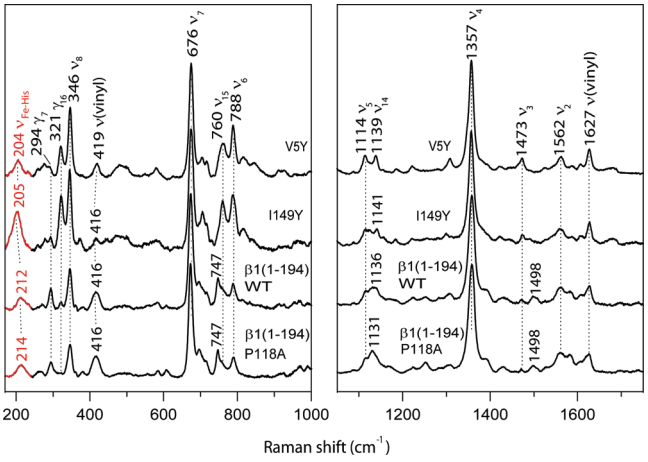

FIGURE 3: 430 nm-excited RR spectra of the ligand-free forms of V5Y and I149Y full-length Fe(II) sGC (top two spectra) and of the WT and P118A β1(1−194) truncate (bottom two spectra). Band assignments (*26*) and frequencies are indicated. The Fe−His stretching bands are highlighted.

by using a low laser power (~0.5 mW at the sample). A single spectrograph (Spex 1269) equipped with a UV-enhanced CCD detector (Princeton Instruments) operating at −110 °C was used to collect the scattered light. UVRR spectra were calibrated using acetone. Grams A/I (Thermo-Galactic) was used to analyze the spectra.

RESULTS

sGC Activity. Included in this study are three variant full-length sGC constructs, with residue substitutions in the heme-binding pocket (Figure 2): P118A, V5Y, and I149Y. All three proteins with these substitutions have lower enzymatic activity in response to the known activators CO and YC-1 (Table 1). Addition of CO to the WT enzyme increases the ligand-free basal activity 2−10-fold, while addition of the effector molecule YC-1 to the Fe(II)−CO complex activates the enzyme an additional 9-fold. The heme pocket mutations produce variable effects on the YC-1-free activities, but all three variants exhibit reduced levels of activation in the presence of YC-1. Specifically, stimulation of the CO adduct by YC-1 is reduced ~3-fold by the P118A and V5Y substitutions and is completely abolished in the I149Y variant.

Ligand-Free RR Spectra. RR spectra of the ligand-free sGC variants (Figure 3) show the usual porphyrin vibrational bands (for mode assignments, see ref *26*) expected for 5-c Fe(II) heme, and also the ν_{Fe-His} band, which is associated with stretching of the bond between the Fe and the proximal histidine ligand. ν_{Fe-His} is found at an unusually low frequency in sGC [204 cm^{-1} (*27*, *28*)], indicating a weakened bond relative to those of other histidine-ligated heme proteins (e.g., 220 cm^{-1} in myoglobin).

The ν_{Fe-His} band is unaffected by the V5Y or I149Y substitution, indicating that the immediate heme environment is similar to that in the wild-type protein. We were unable to record ν_{Fe-His} for the P118A variant of full-length sGC, but this substitution produces a slight upshift (2 cm^{-1}) in ν_{Fe-His} in the truncated heme domain β1(1−194) (Figure 3). The truncation itself, however, produces an elevation of the frequency, from 204 to 212 cm^{-1}, indicating a somewhat strengthened bond when interactions with other domains are absent.

Most of the porphyrin bands in the Fe(II)-unligated RR spectra are not affected by the residue substitutions, except for small changes in relative intensities. The 760 cm^{-1} ν_{15} band is downshifted 13 cm^{-1} in the β1(1−194) truncation when compared to the full-length sGC constructs. Additionally, the 419 cm^{-1} vinyl side chain bending mode observed in sGC V5Y is shifted down 3 cm^{-1} in sGC I149Y, WT β1(1−194), and β1(1−194) P118A. These shifts indicate subtle changes in porphyrin conformation.

Notably, P118A in β1(1−194) has no effect on the porphyrin bands except for the disappearance of a weak 321 cm^{-1} band, identified as the γ_{16} out-of-plane mode. The homologous mutation in the *Tt* H-NOX domain (P115A) relaxes the heme distortion found in the WT structure (*15*). In the RR spectrum of *Tt* H-NOX, this relaxation led to a lower intensity for a number of out-of-plane RR bands in the O_2 complex (*29*). The spectrum of the ligand-free variant *Tt* H-NOX showed no detectable RR changes compared to the WT spectrum except for a slight upshift in the ν_{Fe-His} band, similar to that seen here for β1(1−194) P118A.

RR Spectra of CO Adducts and YC-1 Effects. The CO adducts of WT sGC and the sGC variants were examined by RR spectroscopy. The sGC porphyrin bands undergo characteristic shifts upon CO binding (Figures 4 and 5), and the RR spectra of the CO adducts also exhibit ν_{FeC} and ν_{CO} bands, at ~490 and ~1970 cm^{-1}, respectively, associated with stretching of the Fe−C and C−O bonds of the bound CO. WT sGC has two bands for each of these modes (Figure 4), a dominant pair at 473 and 1985 cm^{-1}, and a weaker pair at 487 and 1969 cm^{-1} [the WT ν_{CO} bands are not shown in Figure 4, since they have been previously reported (*23*, *24*)]. In agreement with earlier studies, addition of YC-1 switches these pairs, so that the 487 and 1969 cm^{-1} bands become dominant. In addition, a new ν_{FeC} band appears at 521 cm^{-1}, characteristic of 5-c Fe(II)heme−CO complex. Thus, we observed that YC-1 binding to the CO adduct leads to the breaking of the Fe−His bond in an unknown fraction of the protein population. These effects are accentuated when the more

potent effector BAY 41-2272 is added to the CO adduct. Specifically, the 521 cm^{-1} band is augmented, and the 473 and 1985 cm^{-1} bands are diminished further in intensity. The ν_{CO} bands are generally weak in RR spectra, making them difficult to deconvolute. However, Martin et al. have shown via infrared spectroscopy (*24*) that the 1969 cm^{-1} band produced by BAY 41-2272 addition to the sGC−CO complex is actually a composite of bands at 1972 and 1964 cm^{-1}. They were able to assign the 1964 cm^{-1} band to the 5-c heme−CO species, on the basis of its temperature dependence.

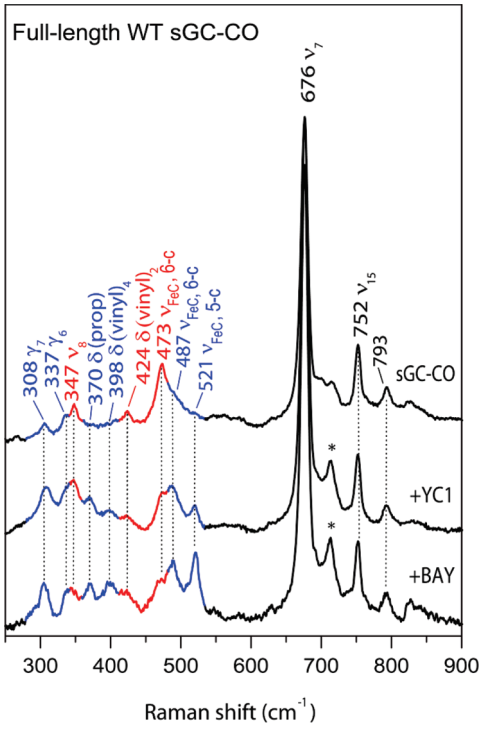

FIGURE 4: WT sGC−CO RR spectral changes produced by YC-1 and BAY 41-2272 with 413 nm excitation. Asterisks denote DMSO bands. Red and blue indicate bands whose relative intensities decrease and increase, respectively, upon effector binding.

In addition, YC-1 decreases the intensity of the 424 cm^{-1} RR band but increases the intensity at 398, 370, and 308 cm^{-1} (Figure 4). BAY 41-2272 again shows the same changes but with greater magnitude. The 424 and 398 cm^{-1} bands are assigned to bending vibrations of the 2- and 4-vinyl heme substituents, respectively; the 370 cm^{-1} band is assigned to a propionate bend, and the 308 cm^{-1} band is likely an out-of-plane porphyrin deformation, γ_7 (*26*). A similar pattern of vinyl and propionate intensity alteration has been seen upon addition of YC-1 to the NO adduct of sGC and was attributed to changes in the tilting of the pyrrole rings to which the vinyl and propionate groups are attached (*30*), producing net planarization of the heme.

The effect of YC-1 on the RR spectra of the sGC variants was also examined. The P118A, V5Y, and I149Y variants have ν_{FeC} bands at 493 cm^{-1}, but P118A and V5Y have a shoulder at 473 cm^{-1}, which decreases upon addition of YC-1 (Figure 5). This shoulder is undetectable for the I149Y variant, with or without YC-1. In the ν_{CO} region, a weak 1988 cm^{-1} band in the P118A spectrum disappears upon addition of YC-1, and the dominant 1969 cm^{-1} band is augmented. A similar effect is seen in the V5Y spectrum, although the frequencies are slightly lower, 1984 and 1960 cm^{-1}, suggesting an influence of the V5Y substitution on the environment of the bound CO. ν_{CO} was undetectable for the I149Y variant because of the low signal-to-noise ratio. Additionally, a split ν_4 in the I149Y spectrum indicates photolysis of the Fe−CO bond occurs both in the presence and in the absence of YC-1.

Significantly, the presence of the 473 cm^{-1} shoulder and its diminution by YC-1 correlate with the degree of activation by YC-1; YC-1-induced activity is greatly diminished in the P118A and V5Y variants and abolished in the I149Y variant (Table 1). To investigate this spectrum−function correlation further, the ν_{FeC} band envelope was deconvoluted and the relative area of the 473 cm^{-1} component was plotted against the relative degree of YC-1 activation of the Fe(II)−CO complex (Table 1 and

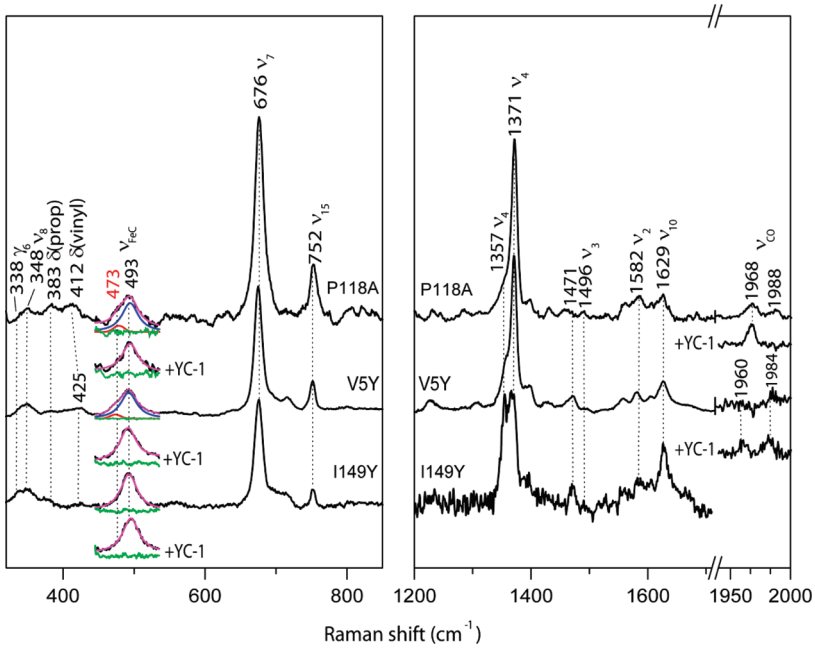

FIGURE 5: 413 nm-excited RR spectra of CO adducts of P118A, V5Y, and I149Y full-length sGC variants and effect of addition of YC-1 on the νFeC and νCO bands (insets). In the insets, black and magenta traces are original and fitted spectra, respectively. Red and blue traces are individual peaks that contribute to the fitted spectrum. The green trace is the residual spectrum (original fit).

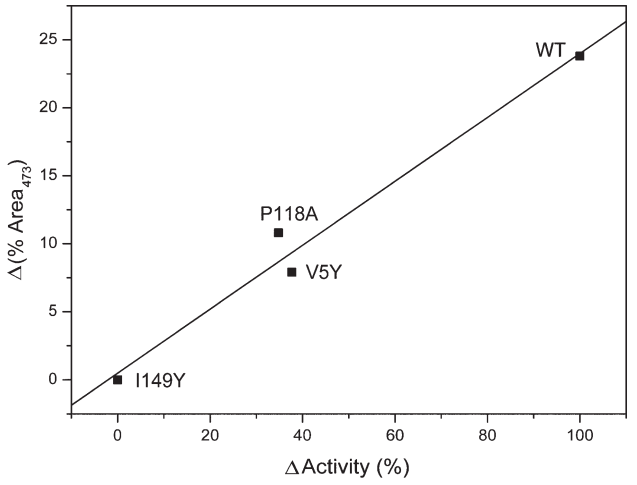

FIGURE 6: Correlation of the ~473 cm^{-1} ν_{FeC} fraction with the relative level of YC-1 activation of the indicated sGC−CO variants.

Figure 6). The straight line defined by WT sGC (100%) and the I149Y variant (0%) passes close to the points for P118A (35%) and V5Y (38%) (Figure 6). Thus, the 473 cm^{-1} ν_{FeC} component represents that fraction of sGC molecules that can be activated by YC-1.

UVRR Spectra of β1(1−385). The heme-binding domain of sGC has a single tryptophan residue, Trp22 (Figures 1 and 2), which appears to be in a region that is responsive to the heme conformation on the basis of a mutational study with *Tt* H-NOX (*15*) (Figure 2). Consequently, we examined the effect of CO and YC-1 binding on the 229 nm-excited UVRR spectrum, in which tryptophan and tyrosine vibrational bands are selectively enhanced (*31*, *32*). The β1(1−385) construct was chosen for this experiment because it has only one tryptophan residue (full-length sGC has five, three in the α1 subunit and two in the β1 subunit) and because it is known (*33*, *34*) to retain the property of having 473 and 1985 cm^{-1} ν_{FeC} and ν_{CO} bands whose intensities are diminished by YC-1.

Figure 7 shows that YC-1 increases the intensity of both tyrosine (Y8a/b, Y9a, and Y7a) and tryptophan (W3, W7, W16, and W17) bands, indicating environmental changes in the aromatic rings. The intensity change suggests that Trp22 becomes less exposed to solvent (*31*) upon addition of YC-1. The tyrosine signals are harder to interpret since β1(1−385) has 14 tyrosine residues.

The UVRR spectrum of ligand-free β1(1−385) (not shown) was indistinguishable from that of the CO adduct, indicating that any CO-induced protein conformation change could not be detected by the aromatic residue probes.

DISCUSSION

Three Spectroscopic States of the sGC−CO Complex Are Linked to Activity. The RR spectral responses to specific sGC variants, and to the binding of effector molecules YC-1 and BAY 41-2272, allow us to identify three states of the sGC−CO complex (Table 2).

State I is associated with the majority population in the WT sGC−CO complex, which has ν_{FeC} and ν_{CO} at 473 and 1985 cm^{-1}, respectively. This population significantly decreases when YC-1 or BAY 41-2272 is added to the WT sGC−CO complex. sGC variants P118A and V5Y have minority populations of state I, which also disappear upon addition of effector, whereas no population of state I is observed in sGC I149Y.

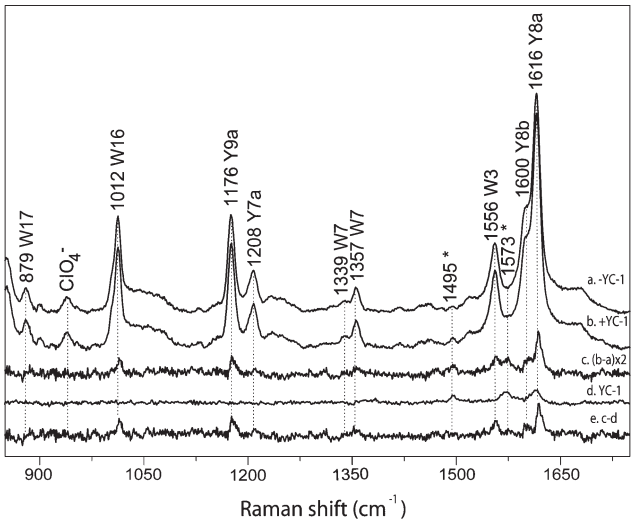

FIGURE 7: 229 nm-excited UVRR spectra of the CO adduct of sGC β1(1−385), before and after addition of YC-1 (a and b, respectively). The YC-1 UVRR spectrum (d) was recorded separately and subtracted from the difference spectrum (c) to yield the intrinsic changes (e) of the protein. In obtaining the difference spectrum (e), we normalized the YC-1 spectrum (d) to spectrum c by equalizing the height of the 1573 cm^{-1} YC-1 band.

Table 2: RR Band Positions for Spectroscopically Defined States of the sGC−CO Complex

state	ν_{FeC} (cm^{-1})	ν_{CO} (cm^{-1})
I	473	1985
II	487, 521[a]	1972, 1964[a,b]
III	493	1968

[a]Five-coordinate heme−CO fraction. [b]IR spectral assignment (*24*).

State II is associated with the majority population when effectors are bound to the sGC−CO complex. A larger state II fraction is induced by BAY 41-2272 than by YC-1. A small state II fraction is already present in the WT sGC−CO complex. State II has a mixture of 6- and 5-c heme−CO adducts, with ν_{FeC} and ν_{CO} at 487 and 1972 cm^{-1} and at 521 and 1964 cm^{-1}, respectively. Although the 6-c fraction appears to be dominant, it is not possible to quantify the ratio of 5- and 6-c fractions, because their molar RR intensities are unknown.

State III is created by the P118A, V5Y, and I149Y mutations; it has ν_{FeC} and ν_{CO} at 493 and 1968 cm^{-1}, respectively, and is unaffected by the addition of effectors. The state III positions are close to those of the 6-c fraction of state II, and the bands cannot readily be deconvoluted. It is possible that the WT sGC−CO complex has a small population of state III as well as a population of state II.

These spectroscopically defined states can be linked to a functional model through the activity data in Table 1. The shift from state I to state II is associated with the shift from low to high activity when YC-1 is added to the sGC−CO complex. Moreover, the extent of state I diminution upon addition of YC-1 correlates quantitatively with the extent of YC-1 activation (Figure 6). Thus, state II represents high-activity enzyme, while state I represents protein that is capable of high activity upon effector binding. It is likely that the modest activity of the effector-free sGC−CO complex reflects the minority state II population that it contains. Meanwhile, state III represents protein that is incapable of being activated by YC-1. Only state

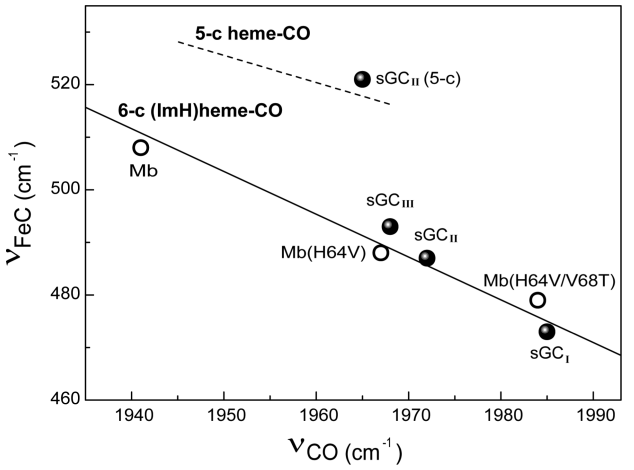

FIGURE 8: Backbonding plot for heme−CO adducts. The dashed and solid lines are published correlations for 5-c heme−CO and for 6-c (ImH)heme−CO adducts, respectively. The empty circles are data (*35*) for myoglobin (Mb) and its H64V (the positively polar distal His is replaced with the nonpolar Val, diminishing the FeCO backbonding) and H64V/V68T (a lone pair donor interaction from the introduced Thr reduces backbonding further) variants. The filled circles are data for sGC in states I, II, and III. sGC_I shows anomalously weak backbonding, while sGC_{II} and sGC_{III} are at positions expected for a hydrophobic heme pocket. sGC_{II} also has a 5-c heme−CO fraction.

III is detectable for the I149Y variant, which is unresponsive to YC-1. State III is dominant for the P118A and V5Y variants, which exhibit a minor state I fraction and a decrease in the level of YC-1-induced activation when compared to that of WT sGC (Figure 6).

Our model suggests that sGC is poised for activation in state I and becomes active in state II. The binding of CO to sGC may produce a small population of state II, while binding of an effector to the sGC−CO complex produces a significant population of state II. However, the required transition from state I to state II can be lost by residue substitutions that alter the structure sufficiently to leave variable fractions of the protein in a form, characterized as state III, that is incapable of being activated.

Structure of the Spectroscopic States. The ν_{FeC} and ν_{CO} frequencies of state I, at 473 and 1985 cm^{-1}, respectively, are unusually low and high, respectively, compared to those of other heme protein−CO adducts. Because of FeCO backbonding, ν_{FeC} and ν_{CO} frequencies are anticorrelated, and the ν_{FeC}/ν_{CO} plot gives information about the influence of protein interactions that affect backbonding (*35*). Figure 8 shows the correlation seen for heme proteins and model complexes having an imidazole ligand *trans* to the CO (6-c) and also for the 5-c CO−heme complex. Shown for illustration are ν_{FeC}/ν_{CO} points for myoglobin (Mb) and for its H64V variant in which the distal His residue, whose NH group provides positive polarity and increases backbonding (*35*), is replaced with a hydrophobic residue. The result of this replacement is to shift the point down the line, the direction of less backbonding. The ν_{FeC}/ν_{CO} points for state III and the 6-c fraction of state II of the sGC−CO complex are close to the H64V variant of Mb, indicating a hydrophobic environment for the bound CO and a normal imidazole *trans* ligand.

The ν_{FeC}/ν_{CO} point for state I also lies on the correlation, indicating an intact Fe−His bond, but at a much lower position, reflective of anomalously weak backbonding. Similarly, weakened backbonding has been detected for the H64V/V68T variant of Mb (Figure 8), in which the introduced threonine side chain is oriented (via H-bonding to a backbone carbonyl) so that its O atom lone pair points at the bound CO (*36*). This orientation weakens backbonding through negative polarity (*35*, *36*). A homology model based on the *Tt* H-NOX structure (Figure 2) suggests that the distal heme pocket in sGC is lined with hydrophobic residues, except for Cys78. The homologous residue in *Tt* H-NOX, Phe78, is sufficiently close to the heme that an introduced OH substituent (F78Y) can donate a H-bond to a heme ligand, as evidenced by restoration of O_2 affinity in a *Tt* H-NOX variant that cannot bind O_2 (Y140L) (*37*, *38*). It is, therefore, conceivable that Cys78 could provide negative polarity to the bound CO in sGC, if the SH group were properly oriented, as the Thr68 OH group is oriented in the H64V/V68T variant of Mb. A structural change upon YC-1 binding could readily abolish the hypothesized Cys78 interaction and shift the ν_{FeC}/ν_{CO} point up the backbonding line to a position characteristic of a hydrophobic pocket, which is seen in state II. Since state III occupies a similar position, one could infer that a different structural change that produces protein incapable of activation also abolishes the interaction of Cys78 with the bound CO. In future studies, the proposed role of Cys78 will be investigated via replacement with apolar residues.

We have recently suggested an alternative explanation for weakened backbonding in the sGC−CO complex, strong H-bonding to the heme propionate substituents (*39*). DFT calculations indicate that neutralization of the propionate negative charges would weaken FeCO backbonding through an inductive effect and would shift the ν_{FeC}/ν_{CO} frequencies by the same magnitude that is observed in the state I-to-state II transition (*39*). The *Tt* H-NOX crystal structure (*14*) shows the propionate groups to be buried and tightly bound to positively charged and H-bond-donating residues. Both propionates interact with Arg135, and one of them accepts H-bonds from Ser133 and Tyr131. These three residues form the YxSxR motif found in all H-NOX domains, including that of the sGC β1 subunit. The shift from state I to state II RR signals could then be explained if YC-1 induces a protein structural change that breaks or weakens these propionate contacts. Again, the near coincidence of state II and state III signals would imply a different, activity-impairing structural change that also weakens the propionate contacts in state III.

A third alternative is that the anomalously low backbonding in state I results from out-of-plane distortion of the heme ring, a prominent feature of the *Tt* H-NOX structure (*14*). In this scenario, the YC-1-induced protein structural change would allow the porphyrin to relax, restoring the backbonding. Again, the activity-impairing structural change in state III would likewise relax the porphyrin distortion. However, relaxation of the porphyrin distortion via the P115A substitution in the *Tt* H-NOX domain was found to have no effect on the ν_{FeC} position in the CO adduct (*29*). This negative result is consistent with earlier DFT calculations (*39*) which predicted insignificant effects of porphyrin distortion on the FeCO vibrational frequencies. The porphyrin distortion is no doubt linked to the propionate contacts, and if the latter are weakened, the porphyrin may well relax. However, it is the propionate contacts that would be the primary determinants of the FeCO frequencies in such a coupled structural change.

A YC-1-induced effect on the heme is also evidenced by the altered intensities of RR bands associated with the peripheral vinyl and propionate substituents in state II (Figure 4). However, these changes are not those expected from simple relaxation of

the porphyrin distortions based on studies with the *Tt* H-NOX domain. Tran et al. (*29*) found that RR changes associated with the heme flattening in the P115A variant involved intensity losses for a number of bands in the 500−1000 cm^{-1} region, which is associated with pyrrole distortion and methine C−H out-of-plane modes. However, the vinyl and propionate mode intensity changes and the γ_7 intensification observed here were not seen with that mutation. Thus, the YC-1-induced changes are not simply due to porphyrin relaxation but must be associated with an enforced geometry change, which produces net planarization. The transition to this altered form results in strengthened FeCO backbonding, due to either a loss of a possible Cys78 lone pair interaction with the CO or weakening of the propionate H-bonds from the YxSxR residues. We note independent evidence from CO and NO rebinding kinetics which shows that YC-1 alters the structure of the heme pocket (*25*, *40*).

The sGC variants examined in this study, which result in a significant population of state III and a reduced level of YC-1 activation, involve the modification of residues in the heme pocket (Figure 2). One of these residues, P118, likely influences the heme via nonbonding interactions and thus may be involved in porphyrin distortion (*15*). The V5Y and I149Y substitutions introduce bulky and polar residues, which may perturb the structure-maintaining heme−protein contacts. Therefore, all three variants may shift the protein to state III by a similar mechanism; however, it remains to be determined if heme distortion is requisite for sGC activation.

Activation Mechanism and Role of Dissociation of the Fe−His Bond. A critical feature of sGC activation by NO is the dissociation of the Fe−histidine bond (*41*), which is induced by the strong *trans* effect of NO when it is bound to Fe(II). This dissociation triggers a conformation change in the protein leading to activation. The weakness of the Fe−His bond in ligand-free sGC, reflected in the low ν_{Fe-His} frequency (Figure 3), suggests that the protein is primed for this dissociation event. In addition, studies of metalloporphyrin binding to apo-sGC have shown significant activity levels when the metal fails to bind histidine [Ni(II) and Cu(II)] (*42*) or when the porphyrin lacks a metal, but no activation occurs when the metal does bind histidine [Fe(II), Co(II), and Mn(II)] (*43*). Similarly, the physiological effect of NO-bound H-NOX protein from *Shewanella oneidensis*, inhibition of a histidine kinase autophosphorylation, is weak for the CO adduct compared to the NO complex (*44*). However, the CO complex of the proximal histidine variant where heme binding is rescued with imidazole has activity approaching that of the NO complex (*16*). The NMR structure of this variant reveals a relaxed heme and a reorientation of the two halves of the H-NOX domain (*16*). Thus, the status of the heme−proximal histidine linkage plays an integral part in structural changes associated with activity in H-NOX domains.

However, it is now known that the stoichiometric binding of NO to sGC activates the enzyme only modestly, in fact to approximately the same extent as CO binding (*8*). The binding of this single molecule of NO results in the dissociation of the Fe−His bond, but clearly, the sGC−NO species is not fully activated. The observation of a low-activity 5-c sGC−NO complex suggests that Fe−His bond dissociation is not sufficient to fully activate sGC, which requires the binding of effectors, or of additional NO (*10*).

On the other hand, the appearance of a 5-c CO−heme signal upon addition of YC-1 to the sGC−CO complex, and its increase

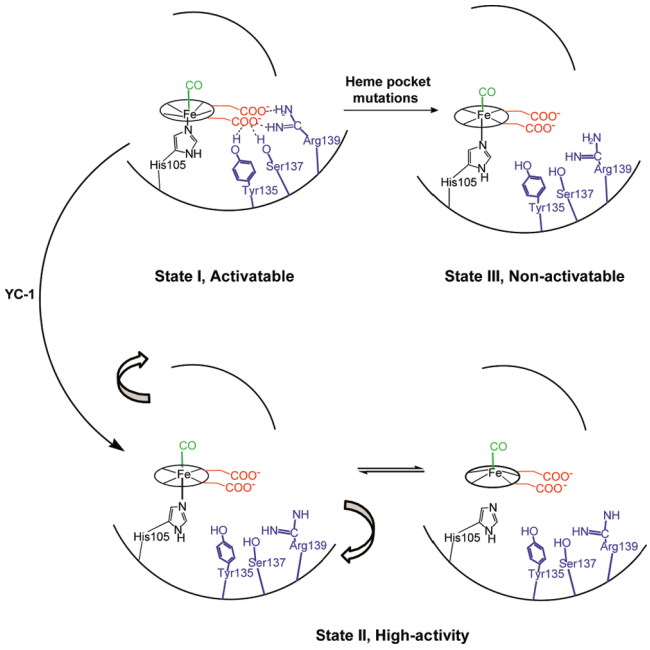

FIGURE 9: Structural model for the activation-linked transitions of the sGC−CO complex. In state I, the binding of CO pulls the Fe toward the heme plane and induces porphyrin distortion via protein contacts. These contacts include strong H-bonds from the YxSxR residues, and possibly from a lone pair interaction of a distal residue, Cys78 (not shown), with the bound CO; either of these contacts might account for the anomalously weak backbonding in state I (see the text). In state III, the protein contacts are loosened, e.g., by residue substitutions in the heme pocket, relaxing the heme and rendering the enzyme incapable of activation. In state II, a hypothesized torque, promoted by effector binding, induces heme planarization, abolishes the YxSxR and/or Cys78 interactions, and breaks the Fe−His105 bond in a fraction of the molecules. The torque is suggested to accompany an activity-inducing rotation of the N-terminal half of the H-NOX domain (*15*). A small population of state II pre-exists in the effector-free CO adduct, likely accounting for its modest activity.

in intensity in the presence of BAY 41-2272, does correlate high-level activation with Fe−His bond dissociation from some of the heme. We infer that formation of state II produces stress on the Fe−His bond and shifts the equilibrium between the 6- and 5-c CO−heme species toward the 5-c form.

Other structural consequences of ligation must also be important. The Fe(II) metal lies out of the heme plane in the resting 5-c state, and it is drawn into the plane by exogenous ligand binding. The heme is held firmly by many nonbonded protein contacts, including the propionate YxSxR interactions mentioned above.

We envision that a torque is applied to the protein as NO or CO draws the Fe(II) toward the distal side (Figure 9). This movement possibly involves a pivot and bend of the heme, as described by Ma et al. for a cyanobacterial H-NOX domain, *Ns* H-NOX (*12*). Through the nonbonded contacts, this torque could be coupled to a large-scale protein displacement, likely similar to the N-terminal displacement seen in the *Tt* H-NOX (*15*) and *Ns* H-NOX (*12*) structures. It is this displacement that the Trp22 UVRR intensities may be sensing (Figure 7). Additionally, this protein displacement could trigger an activating conformational change in the catalytic domain, via interdomain contacts. Through an allosteric interaction, the binding of effector molecules would then increase the torque and therefore the level of activation (state II). However, alterations in the

heme−protein nonbonded contacts, through perturbing residue replacements, would have the effect of slipping the clutch and reducing the attainable torque (state III).

In this scenario, the status of the Fe−His bond is an indicator of the torque level. For NO, the low-level torque produced by ligation is sufficient to break the Fe−His bond, because of the NO *trans* effect, which weakens the Fe−His bond. However, for CO, whose electronic effect is to strengthen the *trans* bond (*45*), the high-level YC-1-induced torque is required to produce partial Fe−His bond dissociation.

ACKNOWLEDGMENT

We thank Rosalie Tran and Richard Mathies for preliminary RR characterization of the Fe(II)-unligated β1(1−194) P118A construct.

NOTE ADDED IN PROOF

Kitagawa and coworkers (*46*) have recently reported similar RR spectral changes upon addition of YC-1 or BAY 41-2272 to sGC-CO, and likewise concluded that effector binding enforces a more planar heme structure. They also suggested reassignment of the 312 cm^{-1} band from an out-of-plane (γ_7) to an in-plane (ν_{52}) mode, consistent with its intensification upon effector binding.

REFERENCES

1. Derbyshire, E. R., and Marletta, M. A. (2009) Biochemistry of soluble guanylate cyclase. In Handbook of Experimental Pharmacology (Schmidt, H. H. H. W., Hofmann, F., and Stasch, J.-P., Eds.) pp 17−31, Springer-Verlag, Berlin.
2. Kots, A. Y., Martin, E., Sharina, I. G., and Murad, F. (2009) A short history of cGMP, guanylyl cyclases, and cGMP-dependent protein kinases. In Handbook of Experimental Pharmacology (Schmidt, H. H. H. W., Hofmann, F., and Stasch, J.-P., Eds.) pp 1−14, Springer-Verlag, Berlin.
3. Ingi, T., Cheng, J., and Ronnett, G. V. (1996) Carbon monoxide: An endogenous modulator of the nitric oxide-cyclic GMP signaling system. *Neuron 16*, 835–842.
4. Ndisang, J. F., Tabien, H. E., and Wang, R. (2004) Carbon monoxide and hypertension. *J. Hypertens. 22*, 1057–1074.
5. Boehning, D., and Snyder, S. H. (2003) Novel neural modulators. *Annu. Rev. Neurosci. 26*, 105–131.
6. Stasch, J.-P., and Hobbs, A. J. (2009) NO-independent, heme-dependent soluble guanylate cyclase stimulators. In Handbook of Experimental Pharmacology (Schmidt, H. H. H. W., Hofmann, F., and Stasch, J.-P., Eds.) pp 277−308, Springer-Verlag, Berlin.
7. Russwurm, M., and Koesling, D. (2004) NO activation of guanylyl cyclase. *EMBO J. 23*, 4443–4450.
8. Cary, S. P. L., Winger, J. A., and Marletta, M. A. (2005) Tonic and acute nitric oxide signaling through soluble guanylate cyclase is mediated by nonheme nitric oxide, ATP, and GTP. *Proc. Natl. Acad. Sci. U.S.A. 102*, 13064–13069.
9. Schmidt, K., Schrammel, A., Koesling, D., and Mayer, B. (2001) Molecular mechanisms involved in the synergistic activation of soluble guanylyl cyclase by YC-1 and nitric oxide in endothelial cells. *Mol. Pharmacol. 59*, 220–224.
10. Fernhoff, N. B., Derbyshire, E. R., and Marletta, M. A. (2009) A nitric oxide/cysteine interaction mediates the activation of soluble guanylate cyclase. *Proc. Natl. Acad. Sci. U.S.A. 106*, 21602–21607.
11. Karow, D. S., Pan, D., Davis, J. H., Behrends, S., Mathies, R. A., and Marletta, M. A. (2005) Characterization of functional heme domains from soluble guanylate cyclase. *Biochemistry 44*, 16266–16274.
12. Ma, X., Sayed, N., Beuve, A., and van den Akker, F. (2007) NO and CO differentially activate soluble guanylyl cyclase via a heme pivot-bend mechanism. *EMBO J. 26*, 578–588.
13. Nioche, P., Berka, V., Vipond, J., Minton, N., Tsai, A. L., and Raman, C. S. (2004) Femtomolar sensitivity of a NO sensor from *Clostridium botulinum*. *Science 306*, 1550–1553.
14. Pellicena, P., Karow, D. S., Boon, E. M., Marletta, M. A., and Kuriyan, J. (2004) Crystal structure of an oxygen-binding heme domain related to soluble guanylate cyclases. *Proc. Natl. Acad. Sci. U.S.A. 101*, 12854–12859.
15. Olea, C., Jr., Boon, E. M., Pellicena, P., Kuriyan, J., and Marletta, M. A. (2008) Probing the function of heme distortion in the H-NOX family. *ACS Chem. Biol. 3*, 703–710.
16. Erbil, W. K., Price, M. S., Wemmer, D. E., and Marletta, M. A. (2009) A structural basis for H-NOX signaling in *Shewanella oneidensis* by trapping a histidine kinase inhibitory conformation. *Proc. Natl. Acad. Sci. U.S.A. 106*, 19753–19760.
17. Russwurm, M., Mergia, E., Mullershausen, F., and Koesling, D. (2002) Inhibition of deactivation of NO-sensitive guanylyl cyclase accounts for the sensitizing effect of YC-1. *J. Biol. Chem. 277*, 24883–24888.
18. Derbyshire, E. R., Fernhoff, N. B., Deng, S., and Marletta, M. A. (2009) Nucleotide regulation of soluble guanylate cyclase substrate specificity. *Biochemistry 48*, 7519–7524.
19. Stasch, J. P., Becker, E. M., Alonso-Alija, C., Apeler, H., Dembowsky, K., Feurer, A., Gerzer, R., Minuth, T., Perzborn, E., Pleiss, U., Schroder, H., Schroeder, W., Stahl, E., Steinke, W., Straub, A., and Schramm, M. (2001) NO-independent regulatory site on soluble guanylate cyclase. *Nature 410*, 212–215.
20. Koglin, M., and Behrends, S. (2003) A functional domain of the α1 subunit of soluble guanylyl cyclase is necessary for activation of the enzyme by nitric oxide and YC-1 but is not involved in heme binding. *J. Biol. Chem. 278*, 12590–12597.
21. Hu, X., Murata, L. B., Weichsel, A., Brailey, J. L., Roberts, S. A., Nighorn, A., and Montfort, W. R. (2008) Allostery in recombinant soluble guanylyl cyclase from *Manduca sexta*. *J. Biol. Chem. 283*, 20968–20977.
22. Hu, X., Feng, C., Hazzard, J. T., Tollin, G., and Montfort, W. R. (2008) Binding of YC-1 or BAY 41-2272 to soluble guanylyl cyclase induces a geminate phase in CO photolysis. *J. Am. Chem. Soc. 130*, 15748–15749.
23. Li, Z., Pal, B., Takenaka, S., Tsuyama, S., and Kitagawa, T. (2005) Resonance Raman evidence for the presence of two heme pocket conformations with varied activities in CO-bound bovine soluble guanylate cyclase and their conversion. *Biochemistry 44*, 939–946.
24. Martin, E., Czarnecki, K., Jayaraman, V., Murad, F., and Kincaid, J. R. (2005) Resonance Raman and infrared spectroscopic studies of high-output forms of human soluble guanylyl cyclase. *J. Am. Chem. Soc. 127*, 4625–4631.
25. Winger, J. A., Derbyshire, E. R., and Marletta, M. A. (2007) Dissociation of nitric oxide from soluble guanylate cyclase and heme-nitric oxide/oxygen binding domain constructs. *J. Biol. Chem. 282*, 897–907.
26. Hu, S., Smith, K. M., and Spiro, T. G. (1996) Assignment of protoheme resonance Raman spectrum by heme labeling in myoglobin. *J. Am. Chem. Soc. 118*, 12638–12646.
27. Deinum, G., Stone, J. R., Babcock, G. T., and Marletta, M. A. (1996) Binding of nitric oxide and carbon monoxide to soluble guanylate cyclase as observed with resonance Raman spectroscopy. *Biochemistry 35*, 1540–1547.
28. Tomita, T., Ogura, T., Tsuyama, S., Imai, Y., and Kitagawa, T. (1997) Effects of GTP on bound nitric oxide of soluble guanylate cyclase probed by resonance Raman spectroscopy. *Biochemistry 36*, 10155–10160.
29. Tran, R., Boon, E. M., Marletta, M. A., and Mathies, R. A. (2009) Resonance Raman spectra of an O_2-binding H-NOX domain reveal heme relaxation upon mutation. *Biochemistry 48*, 8568–8577.
30. Ibrahim, M., Derbyshire, E. R., Soldatova, A. V., Marletta, M. A., and Spiro, T. G. (2010) Soluble guanylate cyclase is activated differently by excess NO and by YC-1: Resonance Raman spectroscopic evidence, manuscript in preparation.
31. Chi, Z., and Asher, S. A. (1998) UV Raman determination of the environment and solvent exposure of Tyr and Trp residues. *J. Phys. Chem. B 102*, 9595–9602.
32. Balakrishnan, G., Weeks, C. L., Ibrahim, M., Soldatova, A. V., and Spiro, T. G. (2008) Protein dynamics from time resolved UV Raman spectroscopy. *Curr. Opin. Struct. Biol. 18*, 623–629.
33. Schelvis, J. P. M., Zhao, Y., Marletta, M. A., and Babcock, G. T. (1998) Resonance Raman characterization of the heme domain of soluble guanylate cyclase. *Biochemistry 37*, 16289–16297.
34. Denniger, J. W., Schelvis, J. P. M., Brandish, P. E., Zhao, Y., Babcock, G. T., and Marletta, M. A. (2000) Interaction of soluble guanylate cyclase with YC-1: Kinetic and resonance Raman studies. *Biochemistry 39*, 4191–4198.
35. Spiro, T. G., Ibrahim, M., and Wasbotten, I. H. (2008) CO, NO and O_2 as vibrational probes of heme protein active sites. In The smallest biomolecules: Diatomics and their interactions with heme proteins (Ghosh, A., Ed.) pp 96−123, Elsevier, Amesterdam.

36. Phillips, G. N., Jr., Theodoro, M. L., Li, T. S., and Olson, J. A. (1999) Bound CO is a molecular probe of electrostatic potential in the distal pocket of myoglobin. *J. Phys. Chem. B 103*, 8817–8829.
37. Boon, E. M., Huang, S. H., and Marletta, M. A. (2005) A molecular basis for NO selectivity in soluble guanylate cyclase. *Nat. Chem. Biol. 1*, 53–59.
38. Boon, E. M., and Marletta, M. A. (2006) Sensitive and selective detection of nitric oxide using an H-NOX domain. *J. Am. Chem. Soc. 128*, 10022–10023.
39. Xu, C., Ibrahim, M., and Spiro, T. G. (2008) DFT analysis of axial and equatorial effects on heme-CO vibrational modes: Applications to CooA and H-NOX heme sensor proteins. *Biochemistry 47*, 2379–2387.
40. Kharitonov, V. G., Sharma, V. S., Magde, D., and Koesling, D. (1999) Kinetics and equilibria of soluble guanylate cyclase ligation by CO: Effect of YC-1. *Biochemistry 38*, 10699–10706.
41. Stone, J. R., and Marletta, M. A. (1996) Spectral and kinetic studies on the activation of soluble guanylate cyclase by nitric oxide. *Biochemistry 35*, 1093–1099.
42. Carr, H. S., Tran, D., Reynolds, M. F., Burstyn, J. N., and Spiro, T. G. (2002) Activation of soluble guanylyl cyclase by four-coordinate metalloporphyrins: Evidence for a role for porphyrin conformation. *Biochemistry 41*, 10149–10157.
43. Dierks, E. A., Hu, S., Yu, A., Spiro, T. G., and Burstyn, J. N. (1997) Demonstration of the role of scission of the proximal histidine-iron bond in the activation of soluble guanylyl cyclase through metalloporphyrin substitution studies. *J. Am. Chem. Soc. 119*, 7316–7323.
44. Price, M. S., Chao, L. Y., and Marletta, M. A. (2007) *Shewanella oneidensis* MR-1 H-NOX regulation of a histidine kinase by nitric oxide. *Biochemistry 46*, 13677–13683.
45. Ibrahim, M., Xu, C.-L., and Spiro, T. G. (2006) Differential sensing of protein influences by NO and CO vibrations in heme adducts. *J. Am. Chem. Soc. 128*, 16834–16845.
46. Pal, B., Tanaka, K., Takenaka, S., and Kitagawa, T. (2010) Resonance Raman spectroscopic investigation of structural changes of CO-heme in soluble guanylate cyclase generated by effectors and substrate. *J. Raman Spectrosc.*, published online January 26, 2010.